

Supporting information - IrOOH nanosheets as acid stable  
electrocatalysts for the oxygen evolution reaction

Daniel Weber<sup>a,b,c</sup>, Leslie M. Schoop<sup>d</sup>, Daniel Wurmbrand<sup>a,e</sup>, Sourav Laha<sup>a</sup>, Filip Podjaski<sup>a,f</sup>,  
Viola Duppel<sup>a</sup>, Kathrin Müller<sup>a</sup>, Ulrich Starke<sup>a</sup>, and Bettina V. Lotsch<sup>a,b,g</sup>

<sup>a</sup>Max Planck Institute for Solid State Research, Heisenbergstrasse 1, 70569 Stuttgart,  
Germany

<sup>b</sup>Ludwig-Maximilians-Universität München, Butenandtstrasse 5-13, 81377 Munich, Germany

<sup>c</sup>Present: Ohio State University, Columbus, USA

<sup>d</sup>Princeton University, Princeton, USA

<sup>e</sup>University of Konstanz, Konstanz, Germany

<sup>f</sup>Ecole Polytechnique Fédérale de Lausanne, Station 12, 1015 Lausanne, Switzerland

<sup>g</sup>Nanosystems Initiative Munich and Center for Nanoscience, Schellingstrasse 4, 80799  
Munich, Germany

*email: b.lotsch@fkf.mpg.de*

**Comment on the synthesis of  $\text{K}_{0.75}\text{Na}_{0.25}\text{IrO}_2$**   $\text{K}_{0.75}\text{Na}_{0.25}\text{IrO}_2$  was synthesized at 900 °C instead of 850 °C, a modification necessary for subsequent exfoliation. The product synthesized at 850 °C could not be converted into nanosheets. At 900 °C, the reactant mixture has a noticeable vapor pressure, which leads to evaporative loss of the product. Thus, the reaction time was optimized to limit evaporation. The modified reaction procedure increases the content of the side phase  $\text{KIr}_4\text{O}_8$  [1] and also leads to the formation of  $\text{Na}_2\text{IrO}_3$ , [2] visible in the PXRD pattern displayed in Fig. S1. The side phases and flux were later removed by acid washing and decantation of the supernatant as well as the centrifugation of the nanosheet dispersion.

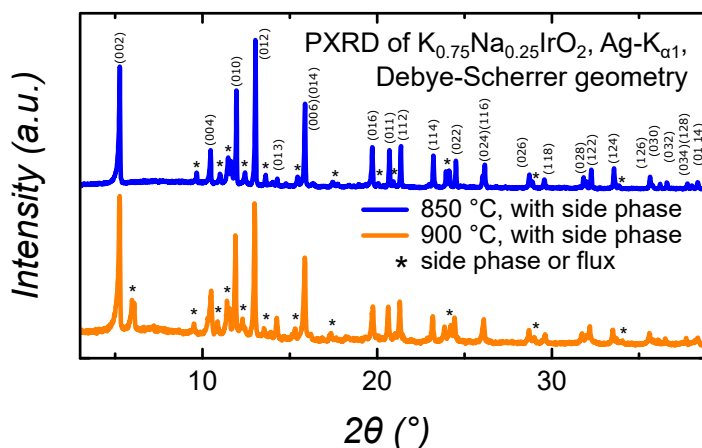


Figure S1: PXRD patterns of  $\text{K}_{0.75}\text{Na}_{0.25}\text{IrO}_2$  synthesized at 850 °C after purification by washing with MeOH (blue), as well as  $\text{K}_{0.75}\text{Na}_{0.25}\text{IrO}_2$  prepared at 900 °C (orange), the main was indexed, asterisks mark reflections of the side phases.

**Synthesis of  $\text{IrOOH}$**  Soaking  $\text{K}_{0.75}\text{Na}_{0.25}\text{IrO}_2$ -900°C in 1 M HCl (1 mL  $\text{mg}^{-1}$  solid) for five days with a daily decantation and exchange of the acid yields exfoliatable bulk  $\text{IrOOH}$ . The resulting flakes and powder had a violet metallic luster. The bulk  $\text{IrOOH}$  reference materials was prepared from  $\text{K}_{0.75}\text{Na}_{0.25}\text{IrO}_2$ -850°C in the same manner, as described in the literature. [3]

**Coverage of nanosheets on Ti substrates** The nanosheet coverage was estimated to be greater than 95 % of the substrate surface from SEM, as only a few spots of different composition were found by BSE. At one of the few areas of low coverage, one of which is depicted in Fig. 3 c) and d), the nanosheets closely followed the rippled surface structure of the Ti substrate observed in Fig. 2 b). With increasing nanosheet film thickness, the film becomes smoother, which suggests that at least several layers lie between the Ti substrate and the IrOOH-air interface.

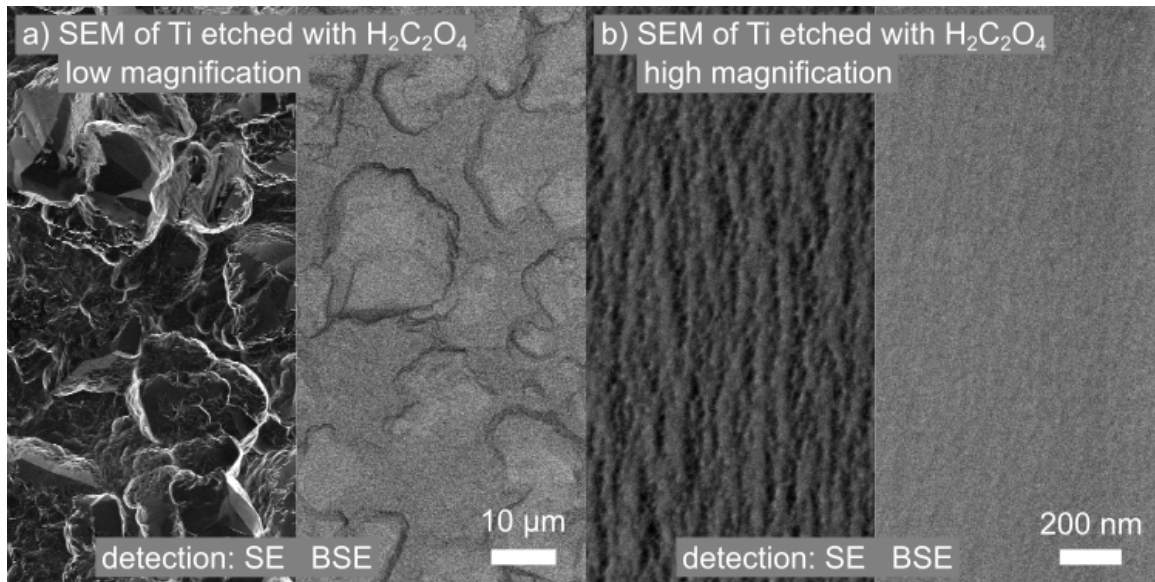


Figure S2: SEM images of H<sub>2</sub>C<sub>2</sub>O<sub>4</sub>-etched Ti substrates with low (a) and high (b) magnification, imaged with SE (left) and BSE (right) detection.

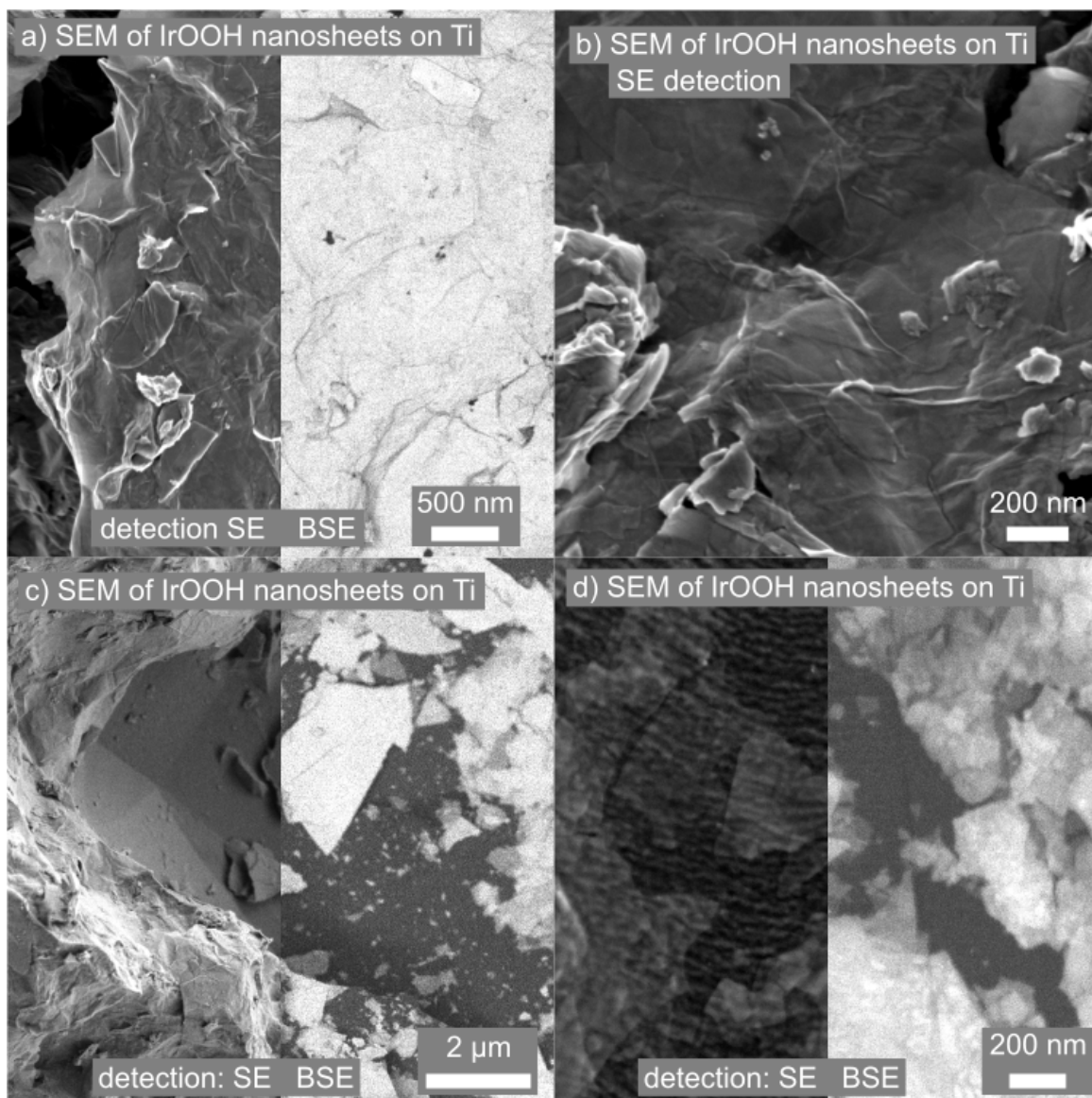


Figure S3: SEM images of various spots with IrOOH nanosheets (BSE: brighter) on etched Ti substrate (BSE: darker), imaged with SE (left) and BSE (right) detection.

**Literature comparison of iridium oxide based catalysts** Table 1 summarizes the electrocatalytic properties of other catalysts systems relevant to this work. As can be observed from the spread of the Tafel slopes and the variations in the overpotential, it is challenging to compare catalytic setups that were not directly measured under the same conditions and/or in the same laboratory.

Table S1: Comparison of  $\eta$  of IrOOH nanosheet electrode to values reported in the recent literature or calculated (\*) from literature data to fit  $j_0 = 10 \text{ mA cm}^{-2}$ .

electrode material	$b$ [mV dec <sup>-1</sup> ] & $\eta$ [V] @ 10 mA cm <sup>-2</sup>	conditions, reference
IrOOH nanosheets	58(3)	0.2 mg cm <sup>-2</sup> loading on Ti, measured
	0.344(7)	at pH = 1 in HClO <sub>4</sub> 0.1 M, this work
IrOOH, bulk	79(3)	0.2 mg cm <sup>-2</sup> loading on Ti, measured
	0.433(5)	at pH = 1 in HClO <sub>4</sub> 0.1 M, this work
IrO <sub>2</sub> , bulk	70(2)	0.2 mg cm <sup>-2</sup> loading on Ti, measured
	0.415(5)	at pH = 1 in HClO <sub>4</sub> 0.1 M, this work
KIr <sub>4</sub> O <sub>8</sub> , bulk	65	0.2 mg cm <sup>-2</sup> loading on Ti,
	0.350	pH = 1 in HClO <sub>4</sub> 0.1 M <sup>[4]</sup>
IrO <sub>2</sub> , bulk	74	0.2 mg cm <sup>-2</sup> loading on Ti,
	0.424	pH = 1 in HClO <sub>4</sub> 0.1 M <sup>[4]</sup>
IrO <sub>2</sub> -(100) $\geq$ 25 nm thick thin film	87 *	PLD grown film on SrTiO <sub>3</sub> -(001),
	0.240 *	pH = 1 in HClO <sub>4</sub> 0.1 M <sup>[5]</sup>
IrO <sub>2</sub> -(110) $\geq$ 25 nm thick thin film	83 *	PLD grown film on BaTiO <sub>3</sub> /MgO
	0.317 *	-(001), pH = 1 in HClO <sub>4</sub> 0.1 M <sup>[5]</sup>
IrO <sub>2</sub> , $\varnothing = 6$ nm nanoparticles	46.5 *	0.05 mg cm <sup>-2</sup> loading, glassy carbon,
	0.350 *	rotating disc, pH = 1 in HClO <sub>4</sub> 0.1 M <sup>[6]</sup>
IrO <sub>2</sub> film, electroflocculated from $\varnothing = 2$ nm nanoparticles	187 *	two data points undefined pH,
	0.493 *	glassy carbon, rotating disc <sup>[7]</sup>
NiFe-LDH nanosheets	40	0.07 mg cm <sup>-2</sup> , pH = 14 in KOH 1 M,
	0.302	glassy carbon electrodes <sup>[8]</sup>
IrO <sub>2</sub> particles	47	0.21 mg cm <sup>-2</sup> , pH = 14 in KOH 1 M,
	0.338	glassy carbon electrodes <sup>[8]</sup>

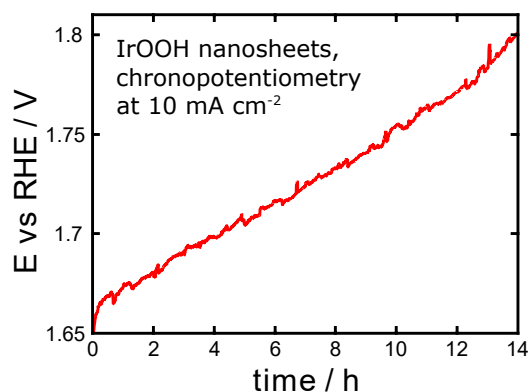


Figure S4: Chronopotentiometry on IrOOH nanosheet electrode at constant current density of  $j = 10 \text{ mA cm}^{-2}$ , catalyst deactivation due to  $\text{O}_2$  gas bubble induced film ablation.

## References

- [1] A. Talanov, W. A. Phelan, Z. A. Kelly, M. A. Siegler, T. M. McQueen, *Inorganic Chemistry* **2014**, *53*, 4500–4507.
- [2] S. K. Choi, R. Coldea, A. N. Kolmogorov, T. Lancaster, I. I. Mazin, S. J. Blundell, P. G. Radaelli, Y. Singh, P. Gegenwart, K. R. Choi, S.-W. Cheong, P. J. Baker, C. Stock, J. Taylor, *Physical Review Letters* **2012**, *108*, 127204.
- [3] D. Weber, L. Schoop, D. Wurmbrand, J. Nuss, E. Seibel, F. F. Tafti, H. Ji, R. J. Cava, R. E. Dinnebier, B. V. Lotsch, *Chemistry of Materials* **2017**, *29*, 8338–8345.
- [4] W. Sun, Y. Song, X.-Q. Gong, L.-m. Cao, J. Yang, *ACS Applied Materials & Interfaces* **2016**, *8*, 820–826.
- [5] K. A. Stoerzinger, L. Qiao, M. D. Biegalski, Y. Shao-Horn, *The Journal of Physical Chemistry Letters* **2014**, *5*, 1636–1641.
- [6] Y. Lee, J. Suntivich, K. J. May, E. E. Perry, Y. Shao-Horn, *The Journal of Physical Chemistry Letters* **2012**, *3*, 399–404.
- [7] T. Nakagawa, C. A. Beasley, R. W. Murray, *The Journal of Physical Chemistry C* **2009**, *113*, 12958–12961.
- [8] X. Long, J. Li, S. Xiao, K. Yan, Z. Wang, H. Chen, S. Yang, *Angewandte Chemie International Edition* **2014**, *53*, 7584–7588.